Ionizable Lipid Nanoparticles with Integrated Immune Checkpoint Inhibition for mRNA CAR T Cell Engineering

*Alex G. Hamilton, Kelsey L. Swingle, Ryann A. Joseph, David Mai, Ningqiang Gong, Margaret M. Billingsley, Mohamad-Gabriel Alameh, Drew Weissman, Neil C. Sheppard, Carl H. June, and Michael J. Mitchell**

The programmed cell death protein 1 (PD-1) signaling pathway is a major source of dampened T cell activity in the tumor microenvironment. While clinical approaches to inhibiting the PD-1 pathway using antibody blockade have been broadly successful, these approaches lead to widespread PD-1 suppression, increasing the risk of autoimmune reactions. This study reports the development of an ionizable lipid nanoparticle (LNP) platform for simultaneous therapeutic gene expression and RNA interference (RNAi)-mediated transient gene knockdown in T cells. In developing this platform, interesting interactions are observed between the two RNA cargoes when co-encapsulated, leading to improved expression and knockdown characteristics compared to delivering either cargo alone. This messenger RNA (mRNA)/small interfering RNA (siRNA) co-delivery platform is adopted to deliver chimeric antigen receptor (CAR) mRNA and siRNA targeting PD-1 to primary human T cells ex vivo and strong CAR expression and PD-1 knockdown are observed without apparent changes to overall T cell activation state. This delivery platform shows great promise for transient immune gene modulation for a number of immunoengineering applications, including the development of improved cancer immunotherapies.

1. Introduction

Chimeric antigen receptor (CAR) T cell therapy has continued to gain traction in recent years as a powerful tool in the clinical arsenal against cancer and other diseases.[1,2] CAR T-based therapies have been approved for the treatment of acute lymphoblastic leukemia (ALL),[3] B cell lymphoma,[4] and multiple myeloma,[5] and are being investigated for use in non-small cell lung cancer,[6] glioblastoma,[7] human immunodeficiency virus (HIV),[8,9] cardiac injury,[10] and others. A major source of the potency of CAR T therapies is the ability of these therapies to harness the patient's own immune system to mount a sophisticated offensive against cancer cells.[11] However, the nature of CAR T therapies as an extension of the immune system means that engineered CAR T cells are susceptible to immunosuppressive signaling in the tumor microenvironment (TME), which hinders the efficacy of CAR T therapies.[12,13]

A. G. Hamilton, K. L. Swingle, R. A. Joseph, D. Mai, N. Gong, M. M. Billingsley, M. J. Mitchell
Department of Bioengineering
University of Pennsylvania
Philadelphia, PA 19104, USA
E-mail: mjmitch@seas.upenn.edu

D. Mai, N. C. Sheppard, C. H. June, M. J. Mitchell
Abramson Cancer Center, Perelman School of Medicine
University of Pennsylvania
Philadelphia, PA 19104, USA

D. Mai, N. C. Sheppard, C. H. June
Center for Cellular Immunotherapies, Perelman School of Medicine
University of Pennsylvania
Philadelphia, PA 19104, USA

M.-G. Alameh, D. Weissman
Department of Medicine
University of Pennsylvania
Philadelphia, PA 19104, USA

M.-G. Alameh, D. Weissman, M. J. Mitchell
Institute for RNA Innovation
University of Pennsylvania
Philadelphia, PA 19104, USA

N. C. Sheppard, C. H. June
Department of Pathology and Laboratory Medicine
Perelman School of Medicine
University of Pennsylvania
Philadelphia, PA 19104, USA

M. J. Mitchell
Institute for Immunology, Perelman School of Medicine
University of Pennsylvania
Philadelphia, PA 19104, USA

M. J. Mitchell
Cardiovascular Institute, Perelman School of Medicine
University of Pennsylvania
Philadelphia, PA 19104, USA

M. J. Mitchell
Institute for Regenerative Medicine, Perelman School of Medicine
University of Pennsylvania
Philadelphia, PA 19104, USA

The ORCID identification number(s) for the author(s) of this article can be found under https://doi.org/10.1002/adhm.202301515

DOI: 10.1002/adhm.202301515

The programmed cell death protein 1 (PD-1) signaling pathway has been established as a major dampener of T cell activity in the TME, including in adoptive CAR T cell therapies.[14,15] PD-1 (CD279), an immune checkpoint receptor, is expressed on the surface of activated T cells.[16] Upon engaging with either of its ligands — programmed cell death ligand 1 (PD-L1) or programmed cell death ligand 2 (PD-L2) — PD-1 initiates an immunosuppressive response, curbing inflammatory T cell activity by promoting apoptosis of effector T cells and inhibiting apoptosis of regulatory T cells.[17,18] While PD-L2 expression is relatively restricted, PD-L1 is overexpressed in a wide variety of cancers and is thought to play a major role in immune evasion generally and in decreased CAR T cell efficacy specifically.[15,17] Inhibition of interactions between PD-1 and PD-L1 is therefore of great interest as a potential means to rescue CAR T efficacy in PD-L1-rich TMEs.[19]

Blockade of PD-1 and/or its ligands using blocking antibodies is a widely used clinical strategy for overcoming the immunosuppressive PD-1 pathway.[20] While combining blocking antibodies with CAR T cell therapy is a useful approach, administration of free antibody leads to widespread suppression of PD-1 signaling, with the potential for autoimmune responses.[19,21] As CAR T therapy already requires the engineering of autogenic T cells to express the exogenous CAR, there is the potential to incorporate targeted PD-1 inhibition to produce CAR T cells with inhibited PD-1 signaling while leaving the PD-1 pathway intact elsewhere. This approach of disrupting the PD-1 pathway concomitantly with CAR engineering has been investigated with promising results using several approaches, including CRISPR-Cas9-mediated knockout of PD-1,[22–24] integration of an engineered soluble anti-PD-1 single-chain variable fragment (scFv),[25] and expression of short hairpin RNA (shRNA) targeting PD-1.[15] However, most of these approaches rely on alteration of the genome through viral gene delivery and/or CRISPR-Cas9 genome editing. This means that these PD-1 inhibition measures are permanent, creating T cells that are permanently desensitized to this anti-inflammatory signaling pathway, opening the door to autoimmune reactions. However, T cells are equipped with an endogenous mechanism for transient suppression of genetic transcripts using the RNA-induced silencing complex (RISC). Transient disruption of the PD-1 signaling pathway at the transcriptome level using RNA interference (RNAi) therefore provides an attractive and underexplored alternative to current approaches.

Our group has recently reported the development of a non-viral platform for the production of transient CAR T cells through the delivery of CAR-encoding messenger RNA (mRNA) using ionizable lipid nanoparticles (LNPs).[26,27] In the present work, we augment this platform to enable simultaneous expression of exogenous mRNA and transient disruption of arbitrary endogenes using RNAi. We use the engineered LNP platform to deliver CAR mRNA and small interfering RNA (siRNA) targeting PD-1 to T cells ex vivo, generating human T cells with potent but transient CAR expression and temporary cell-intrinsic PD-1 disruption. These "super" CAR T cells, after performing their function, can return to function as normal patient T cells, greatly limiting the scope of off-target effects due to both CAR expression and PD-1 inhibition. We further report results showing interesting interplay between mRNA and siRNA cargoes resulting from co-encapsulation, suggesting that incorporation of siRNA may be beneficial for LNP-mediated mRNA delivery even in applications not requiring gene silencing.

2. Results and Discussion

2.1. Ionizable Lipid Synthesis and LNP Formulation

To develop LNPs for co-delivery of mRNA and siRNA to T cells, we formulated LNPs with four main lipid components (**Figure 1**b). These components are an ionizable lipid, essential for endosomal escape and the release of cargo into the cytosol; "helper" phospholipid, which aids in encapsulation and LNP membrane formation; cholesterol, which lends to membrane stability and fusion; and lipid-anchored poly(ethylene glycol) (PEG), which prolongs circulation and limits interactions with the innate immune system.[28–31] We used the novel ionizable lipid C14-494, previously referred to as "C14-4," for all LNP formulations in the present study, as LNPs using this lipid have previously demonstrated potent mRNA delivery to T cells in vitro and ex vivo.[26,27] To produce the C14-494 ionizable lipid, we reacted the 494 polyamine core with excess 14-carbon alkyl epoxide tails, with product identity and purity confirmed by liquid chromatography-mass spectrometry (LC-MS) (Figure 1a; Figure S1, Supporting Information).[26,32] We investigated two "helper" lipids in this study: 1,2-dioleoyl-*sn*-glycero-3-phosphoethanolamine (DOPE), which is commonly used in LNP formulations for mRNA delivery; and 1,2-distearoyl-*sn*-glycero-3-phosphocholine (DSPC), which has historically been used for siRNA encapsulation.[28,32] To formulate LNPs, we combined all lipid components in ethanol and mixed them with an aqueous phase containing mRNA and/or siRNA using a microfluidic device fabricated with staggered herringbone mixers as described previously (Figure 1b).[33,34] Following formulation, we characterized LNP hydrodynamic size, polydispersity, zeta potential, ionizability, and RNA entrapment using standard methods. We observed apparent LNP p*Ka*values between five and seven, suggesting ionizability in the late endosome (Figure 1c). LNPs were generally monodisperse, with diameters generally below 100 nm (Figure 1d).

2.2. Screening Excipient Compositions for Dual RNA Delivery In Vitro

To develop LNPs for dual RNA delivery to T cells, we first turned our attention to tuning the composition of LNPs to accommodate a mixed cargo of mRNA and siRNA. To this end, we designed a library of LNPs with excipient combinations varying along a continuum from "siRNA-like" to "mRNA-like" based on a previous study (**Table 1**).[35] While this prior study identified excipient compositions for co-delivery of mRNA and siRNA, we reasoned that delivery optima might vary based on cell type and ionizable lipid structure, as ionizable lipid structure has been shown to have dramatic effects on transfection characteristics of LNPs and the novel ionizable lipid C14-494 possesses a substantially different chemical structure than previously-investigated ionizable lipids for dual RNA delivery.[35–37]

To probe the effects of excipient makeup on in vitro RNA co-delivery to T cells, we co-encapsulated mRNA encoding mCherry

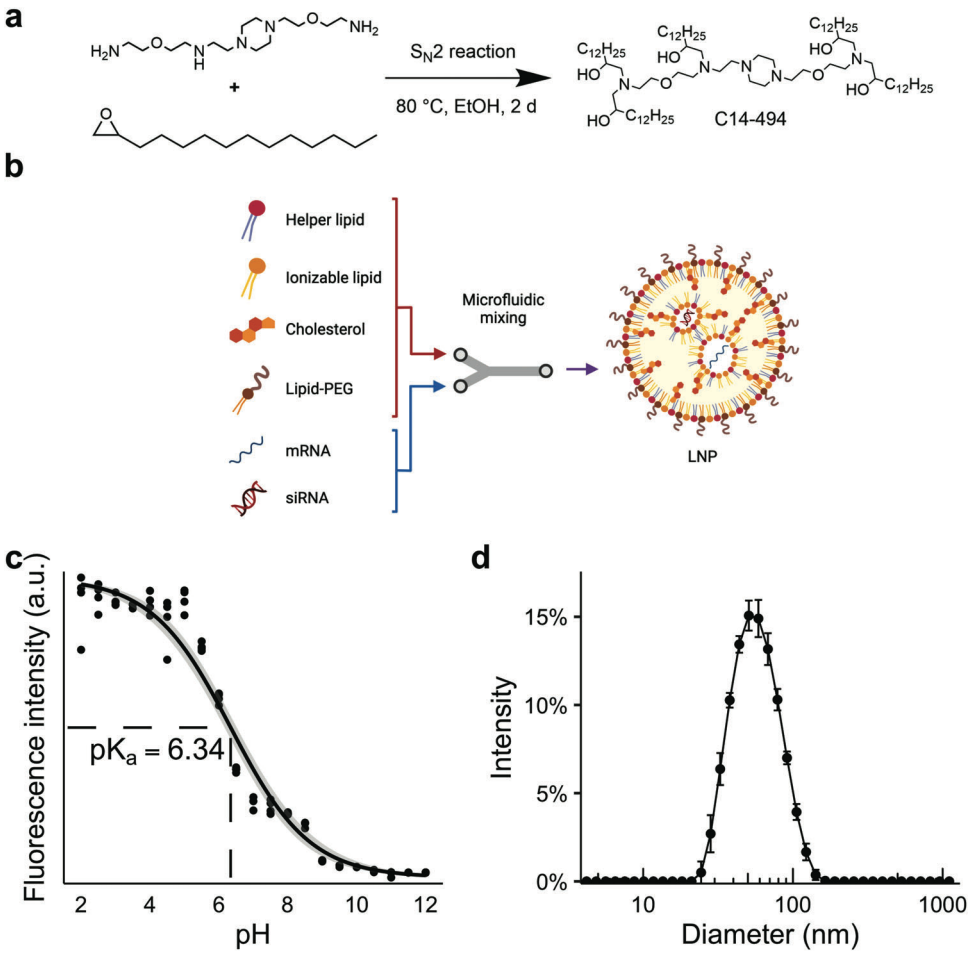

Figure 1. a) S_N2 reaction scheme used to produce the ionizable lipid C14-494 used in this study. b) Overview of LNP fabrication via microfluidic mixing, showing the four commonly used lipid components: ionizable lipid, "helper" phospholipid, cholesterol, and lipid-anchored PEG. LNPs were formulated by placing mRNA and/or siRNA in an aqueous buffer and mixing organic and aqueous phases to promote LNP self-assembly. c) Representative TNS plot from co-encapsulating LNPs demonstrating their ionizability ($5 < pK_a < 7$). d) Representative DLS plot from co-encapsulating LNPs.

Table 1. Excipient compositions screened in Jurkat cells in vitro for dual RNA delivery. The W1 formulation is representative of typical LNP formulations for siRNA delivery, whereas the W5 formulation is representative of typical mRNA LNP formulations. Excipients were varied to probe the design space between these two extremes (formulations W2–W4).

Formulation	W1	W2	W3	W4	W5
Ionizable lipid:nucleic acid weight ratio	5:1	6.25:1	7.5:1	8.75:1	10:1
Ionizable lipid (%mol)	50.0	46.3	42.5	38.8	35.0
DSPC (%mol)	10.0	8.6	6.5	3.6	0.0
DOPE (%mol)	0.0	2.9	6.5	10.9	16.0
Cholesterol (%mol)	38.5	40.5	42.5	44.5	46.5
C14-PEG2000 (%mol)	1.5	1.75	2.0	2.25	2.5

and siRNA targeting enhanced green fluorescent protein (EGFP) in LNPs of varying excipient composition (Table 1). Characterization revealed that LNP hydrodynamic diameter was generally higher in "siRNA-like" formulations than in "mRNA-like" formulations (**Figure 2**a). All observed *z*-average diameters were below 150 nm, and nearly all polydispersity indices (PdIs) were below 0.3, with a single exception (Figure S2, Supporting Information). Notably, RNA entrapment was much higher in formulations containing DOPE — formulation W1, containing only DSPC as its phospholipid, displayed 63.8% ± 1.0% entrapment efficiency, while all other formulations demonstrated mean entrapment efficiencies of at least 88% (Figure 2d). Of particular note, formulations W4 and W5, the most "mRNA-like" formulations, achieved mean entrapment efficiencies up to 97% and approximately 6× greater mean encapsulated RNA concentrations than formulation W1 (Figure 2c,d). Zeta potential was moderately negative for formulation W1 (mean −13.9 mV), perhaps due to its relatively poor encapsulation of RNA, but became steadily more positive with increasing entrapment efficiency, reaching a slight positive (mean 6.35 mV) in formulation W5 (Figure 2b).

For convenience, we began our investigation into T cell nucleic acid co-delivery using Jurkat cells — a well-established immortalized human T cell line commonly used in immunological models.[38] We treated Jurkat cells stably expressing EGFP with LNPs containing mCherry mRNA and EGFP siRNA at a dose of 50 ng of encapsulated mRNA per 100,000 cells. 1 d later, we quantified mCherry and EGFP fluorescence as measures of mRNA

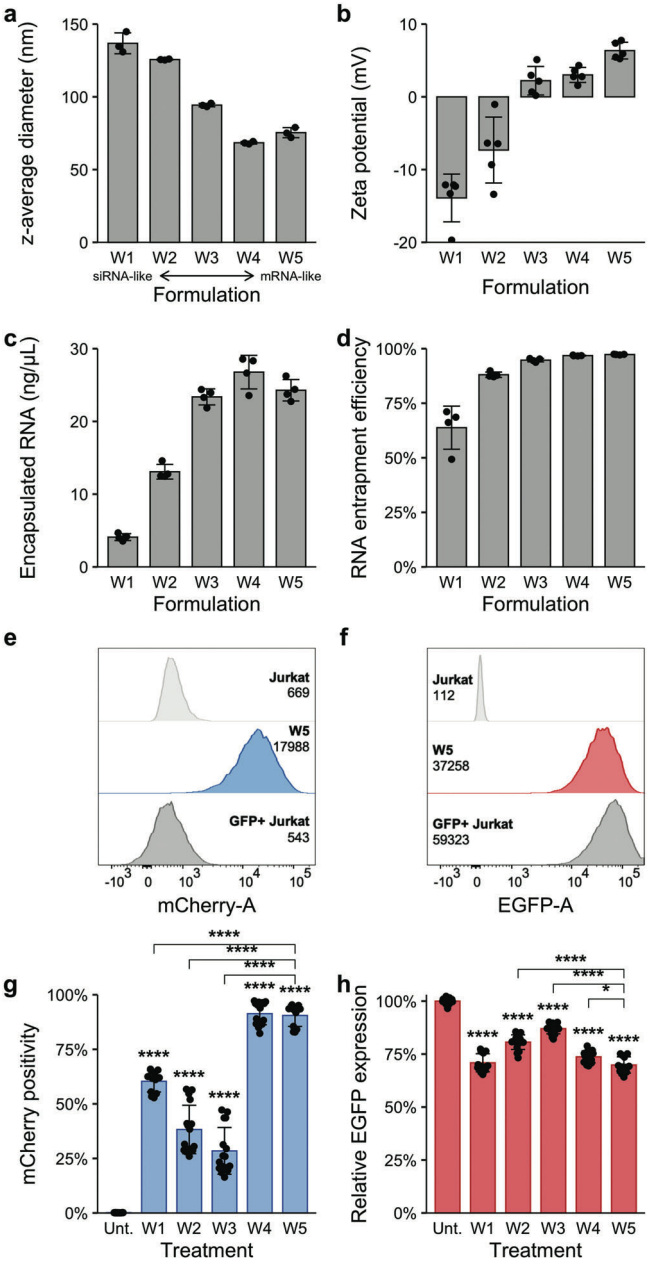

Figure 2. a) *z*-average diameter, b) zeta potential, c) encapsulated RNA content, and d) RNA entrapment efficiency of LNPs formulated with varying excipient compositions. Data are presented as mean ± standard deviation ($n \geq 3$ observations). Representative histograms of e) mCherry and f) EGFP expression measured by flow cytometry following treatment with W5 LNPs co-encapsulating mCherry mRNA and EGFP siRNA, with median fluorescent intensities indicated. g) mCherry expression and h) relative EGFP expression of EGFP$^+$ Jurkat cells treated with LNPs co-encapsulating mCherry mRNA and EGFP siRNA at a dose of 50 ng of encapsulated mRNA per 100,000 cells (6 ng of encapsulated siRNA per 100,000 cells). *: $p < 0.05$, ****: $p < 0.0001$. Statistical annotations without brackets represent comparisons to untreated cells; annotations with brackets indicate comparisons to formulation W5, which was selected as the lead formulation. Data are presented as mean ± standard deviation ($n = 12$ observations).

Table 2. Nucleic acid combinations tested in vitro in Jurkat cells for dual RNA delivery. Formulation X1 served as an mRNA control, while formulation X6 acted as an siRNA control. The excipients used for all formulations in library X were based on formulation W5.

Formulation	X1	X2	X3	X4	X5	X6
mRNA mass (μg)	25	25	25	25	25	0
siRNA mass (μg)	0	1.5	3	5	10	20

delivery and siRNA delivery, respectively, using flow cytometry, with secondary confirmation using fluorescence microscopy (Figure 2e–h; Figures S4 and S5, Supporting Information). We quantified EGFP knockdown through comparison to untreated EGFP$^+$ Jurkat cells and untreated wild-type (EGFP$^-$) Jurkat cells; we assessed mCherry expression as positivity rate through comparison to untreated wild-type Jurkat cells. This screen identified formulations W4 and W5 as mediating the greatest functional delivery of both mRNA and siRNA in vitro, with mCherry positivity rates of 91.4% ± 5.1% and 90.5% ± 5.0% and apparent EGFP knockdown amounts of 26.3% ± 2.8% and 30.1% ± 3.9%, respectively. Importantly, proteomic measurements of EGFP knockdown may underestimate the actual transcriptomic effects of siRNA delivery; however, this only affects attempts at absolute quantification and does not diminish the use of proteomic measurements as a proxy for relative siRNA delivery. Because of the superior knockdown characteristics of formulation W5, the indistinguishable mRNA delivery between the two lead formulations, and the relative simplicity of formulation W5 — comprising only four excipients as opposed to W4's five excipients — we selected the excipient composition of formulation W5 for further optimization.

2.3. Influence of Nucleic Acid Cargo Composition on Dual RNA Delivery In Vitro

A previous investigation of co-transfection with mRNA and siRNA has suggested that the presence and relative amount of each type of nucleic acid may influence the delivery of the other.[35] To characterize the effects of cargo composition on delivery, we designed and fabricated LNPs containing a fixed amount of mCherry mRNA but variable amounts of EGFP siRNA, along with an siRNA control containing only EGFP siRNA (**Table 2**). Characterization revealed generally favorable physicochemical characteristics for these LNPs, with all mean *z*-average diameters observed below 100 nm and generally slightly positive zeta potentials (Figure S3, Supporting Information). We then used these LNPs to transfect Jurkat cells stably expressing EGFP. To probe the effects of relative mRNA amount on siRNA delivery, we treated cells at a fixed dose of 2 ng of siRNA per 100,000 cells. To investigate the effects of relative siRNA amount on mRNA delivery, we separately treated cells at a fixed dose of 33.3 ng of mRNA per 100,000 cells. 24 h later, we measured mCherry and EGFP fluorescence using flow cytometry, determining positivity rates and knockdown amounts by comparison to untreated EGFP$^+$ and wild-type Jurkat cells and confirming transfection with fluorescence microscopy (**Figure 3**; Figures S6 and S7, Supporting Information). Interestingly, mRNA content seemed to modestly influence siRNA-mediated knockdown, with a moderate amount

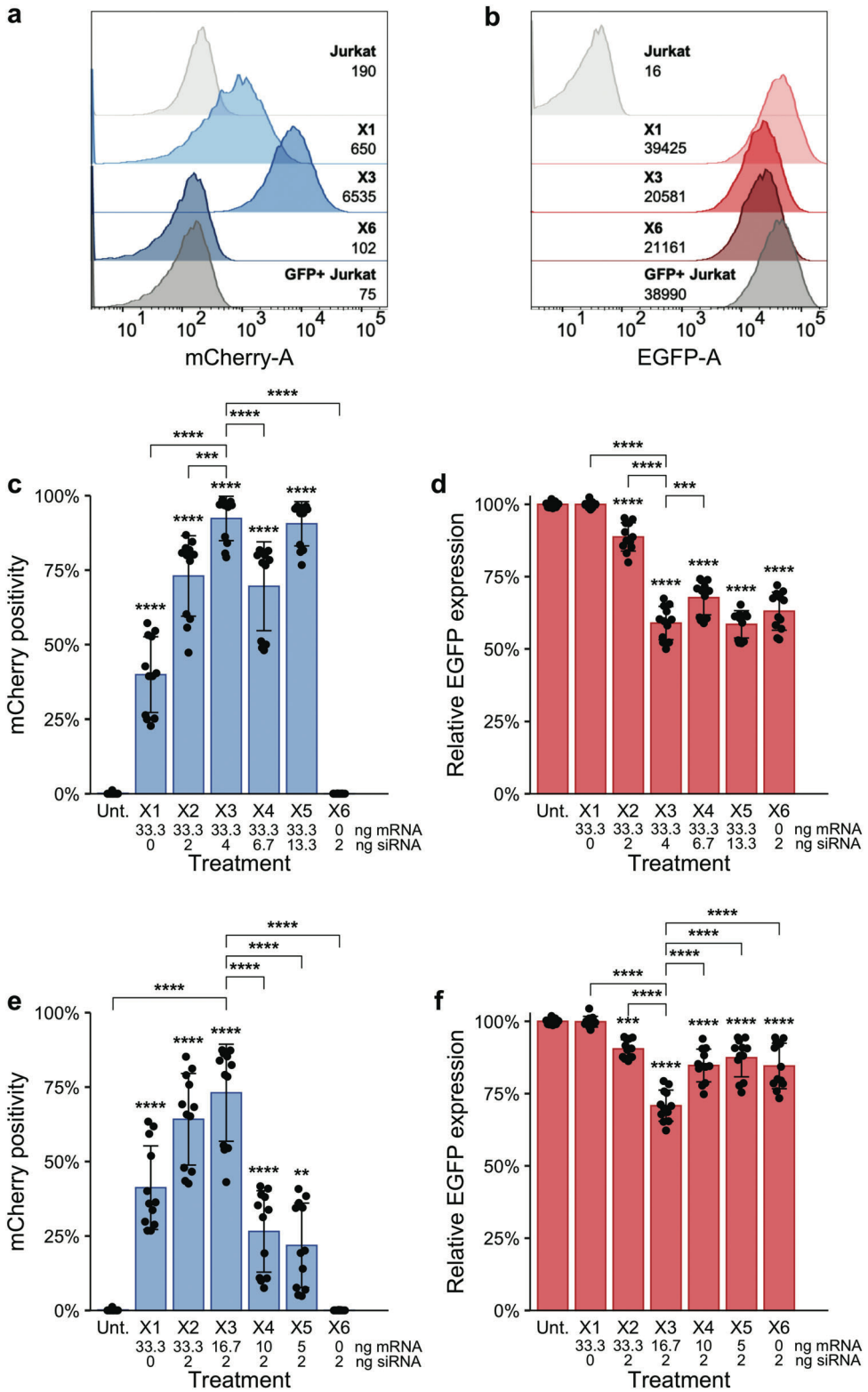

Figure 3. Representative histograms of a) mCherry and b) EGFP expression in EGFP$^+$ Jurkat cells treated with LNPs co-encapsulating mCherry mRNA and EGFP siRNA (X3), only mCherry mRNA (X1), or only EGFP siRNA (X6). Listed values indicate median fluorescent intensities. c,e) mCherry and d,f) EGFP expression in EGFP$^+$ Jurkat cells treated with LNPs co-encapsulating varying ratios of mCherry mRNA and EGFP siRNA c,d) at a fixed amount of mRNA or e,f) at a fixed amount of siRNA. *: $p < 0.05$, **: $p < 0.01$, ****: $p < 0.0001$. Statistical annotations without brackets represent comparisons to untreated cells; annotations with brackets indicate comparisons to formulation X3, which was selected as the lead formulation. Data are presented as mean ± standard deviation ($n = 12$ observations).

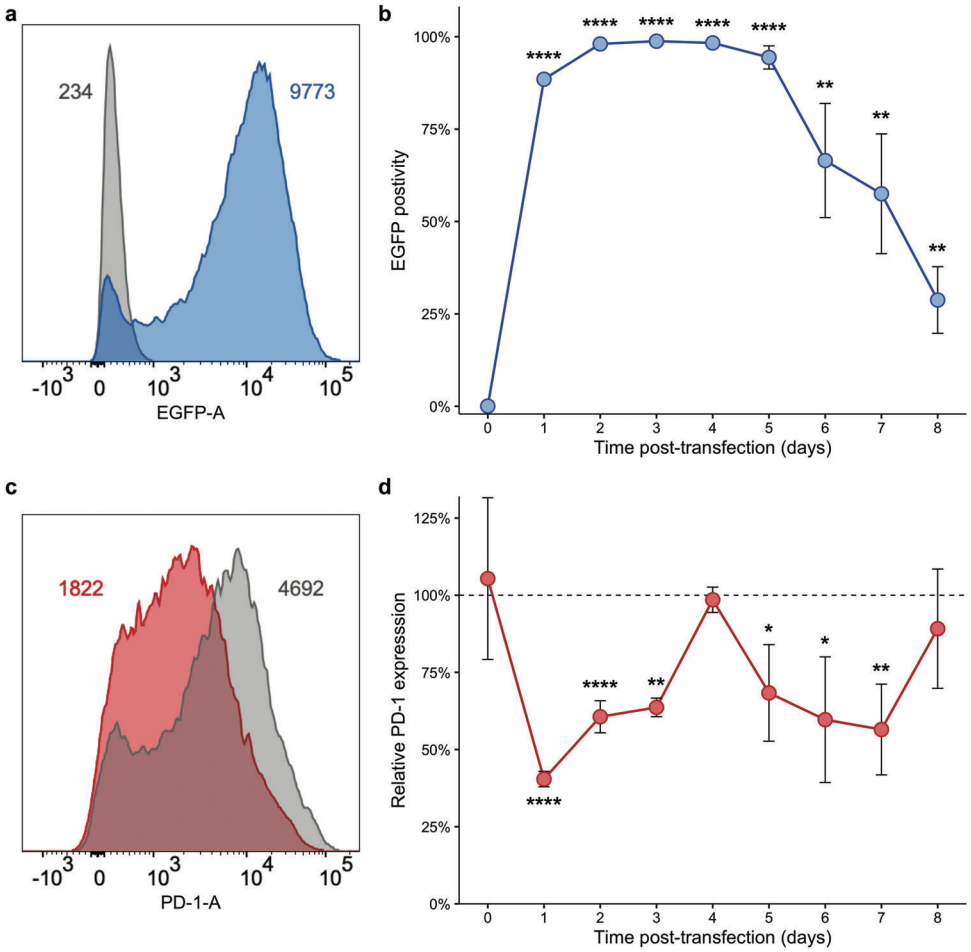

Figure 4. a) Representative histogram showing degree of EGFP expression 1 d after transfection with LNPs co-encapsulating EGFP mRNA and PD-1 siRNA, with median fluorescent intensities indicated. b) EGFP expression over time in primary human T cells treated with dual-encapsulating LNPs. c) Representative histogram showing degree of PD-1 knockdown 1 d after transfection with LNPs co-encapsulating EGFP mRNA and PD-1 siRNA, with median fluorescent intensities indicated. d) Relative PD-1 expression over time in primary human T cells treated with dual-encapsulating LNPs. Cells were treated at a dose of 300 ng of mRNA per 100,000 cells. *: $p < 0.05$, **: $p < 0.01$, ****: $p < 0.0001$. Statistical annotations indicate comparisons to untreated T cells on the corresponding day of the study. Data are presented as mean ± standard deviation ($n = 4$ observations).

of additional mRNA bolstering the inhibitory effect of LNPs compared to the siRNA control LNP X6 (Figure 3b,f). Specifically, the siRNA control formulation X6 demonstrated EGFP knockdown of 15.4% ± 7.9%, while the mRNA-containing formulation X3 displayed EGFP knockdown of 29.2% ± 5.4% at a fixed siRNA dose of 2 ng per 100,000 cells. Similarly, increasing siRNA content substantially improved mRNA delivery to a point, after which additional siRNA had little effect on mRNA expression, consistent with a previous report (Figure 3a,c).[35] The mRNA control formulation X1 achieved 39.9% ± 12.7% mCherry transfection, while the siRNA-containing formulation X3 attained a remarkable 92.4% ± 7.5% transfection at a fixed mRNA dose of 33.3 ng per 100,000 cells. Formulation X3, which was formulated using an mRNA:siRNA weight ratio of 25:3 and demonstrated both the greatest knockdown and the greatest mRNA expression of all formulations tested, emerged from this study as the lead LNP formulation for T cell co-delivery and was consequently used as the basis for LNPs encapsulating therapeutic RNAs.

2.4. Kinetics of Ex Vivo PD-1 Knockdown in Primary Human T Cells

To verify PD-1 knockdown in primary human cells following treatment with PD-1 siRNA and identify conditions suitable for subsequent studies, we performed an ex vivo PD-1 knockdown kinetics study. We used readily-available EGFP mRNA as a stand-in for CAR mRNA for kinetics studies. We co-encapsulated EGFP mRNA with siRNA targeting human PD-1 in LNPs using the excipient composition and nucleic acid ratio identified through in vitro screening (formulation X3). We activated primary human T cells overnight, then treated them at an mRNA dose of 300 ng of encapsulated mRNA per 100,000 cells. Immediately following transfection and daily for the following 8 d, we quantified EGFP and PD-1 expression using flow cytometry (**Figure 4**). EGFP expression data revealed strong mRNA expression starting 1 d post-transfection, with maximal expression — corresponding to nearly 99% transfection — occuring 2 d following transfection

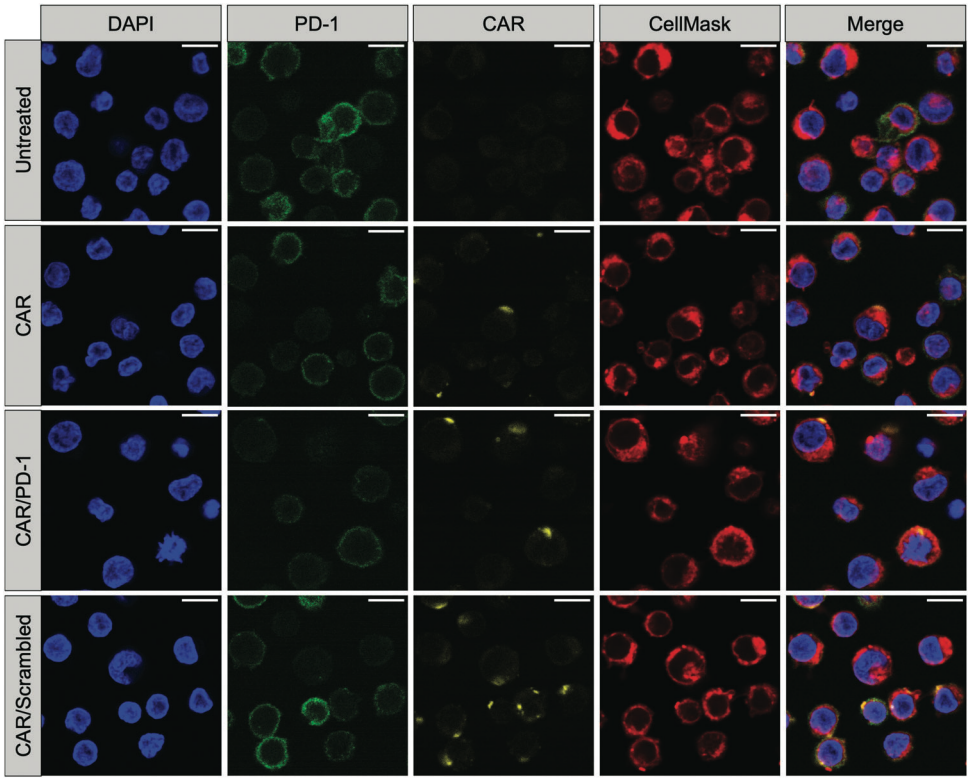

Figure 5. Representative images from confocal laser scanning microscopy of primary human T cells treated with LNPs encapsulating CAR mRNA, CAR mRNA and PD-1 siRNA, or CAR mRNA and scrambled siRNA at a dose of 500 ng of encapsulated CAR mRNA per 100,000 cells. Images were acquired with a 20× objective. Scale bar: 10 µm.

(Figure 4a,b). Remarkably, this expression was quite durable, with fluorescence detection lasting for the entirety of the 8-d study. However, due to the relatively long cytosolic half-life of EGFP — on the order of 1 d — it is difficult to determine for precisely how long mRNA translation occurred.[39] Moreover, PD-1 expression data showed strong and persistent siRNA-mediated PD-1 knockdown, with the maximal reduction — roughly 60% — occurring 1 d post-transfection (Figure 4c,d). We observed a brief return to baseline levels of PD-1 expression 4 d post-transfection, which may warrant further exploration to improve understanding of checkpoint receptor expression in CAR T manufacturing. Nonetheless, we noted PD-1 knockdown up to 7 d post-transfection, in close accordance with our mRNA expression duration. This synchronization of CAR expression and PD-1 suppression is desirable to achieve immune checkpoint desensitization during the critical window of CAR efficacy while minimizing risks of off-tumor autoimmunity after CAR expression fades through the restoration of immune checkpoint interactions. Based on the observed translation and knockdown characteristics 1 d post-transfection, we selected this time point for subsequent experiments.

2.5. Ex Vivo Engineering of PD-1^{lo} Human CAR T Cells

With dose and time parameters for primary cell experiments established, we next performed therapeutic gene expression assays. We activated primary human T cells overnight and treated them with LNPs (formulation X3) encapsulating nucleoside-modified cap 1 CAR mRNA and PD-1 siRNA at a dose of 500 ng of encapsulated mRNA per 100,000 cells. We also included LNPs encapsulating only CAR mRNA and LNPs encapsulating CAR mRNA and scrambled siRNA as controls. The following day, to confirm CAR expression, we prepared samples for fluorescence imaging, staining for cell nuclei and membranes and surface CAR and PD-1 expression and acquiring images using confocal laser scanning microscopy (CLSM). CAR expression was detected in all treated samples (**Figure 5**), with an apparent qualitative increase in CAR expression in groups treated with dual-encapsulating LNPs.

Following confirmation of CAR expression, we again activated cells overnight and treated them with LNPs encapsulating CAR mRNA, CAR mRNA and PD-1 siRNA, or CAR mRNA and scrambled siRNA. The following day, we assessed CAR and PD-1 expression via flow cytometry. We simultaneously measured the expression of activation markers CD25, CD62L (L-selectin), and CD69, as well as T cell markers CD3, CD4, and CD8 (**Figure 6**). Strikingly, we observed very strong CAR expression — up to nearly 71% transfection — which in all cases appeared bolstered by the inclusion of siRNA, consistent with results from reporter gene experiments and observations from microscopy and representing a substantial improvement in CAR-T engineering efficiency compared to previous reports (Figure 6a,b).[26,27] T cells treated with LNPs encapsulating CAR mRNA alone demonstrated 49.4% ± 5.7% transfection among

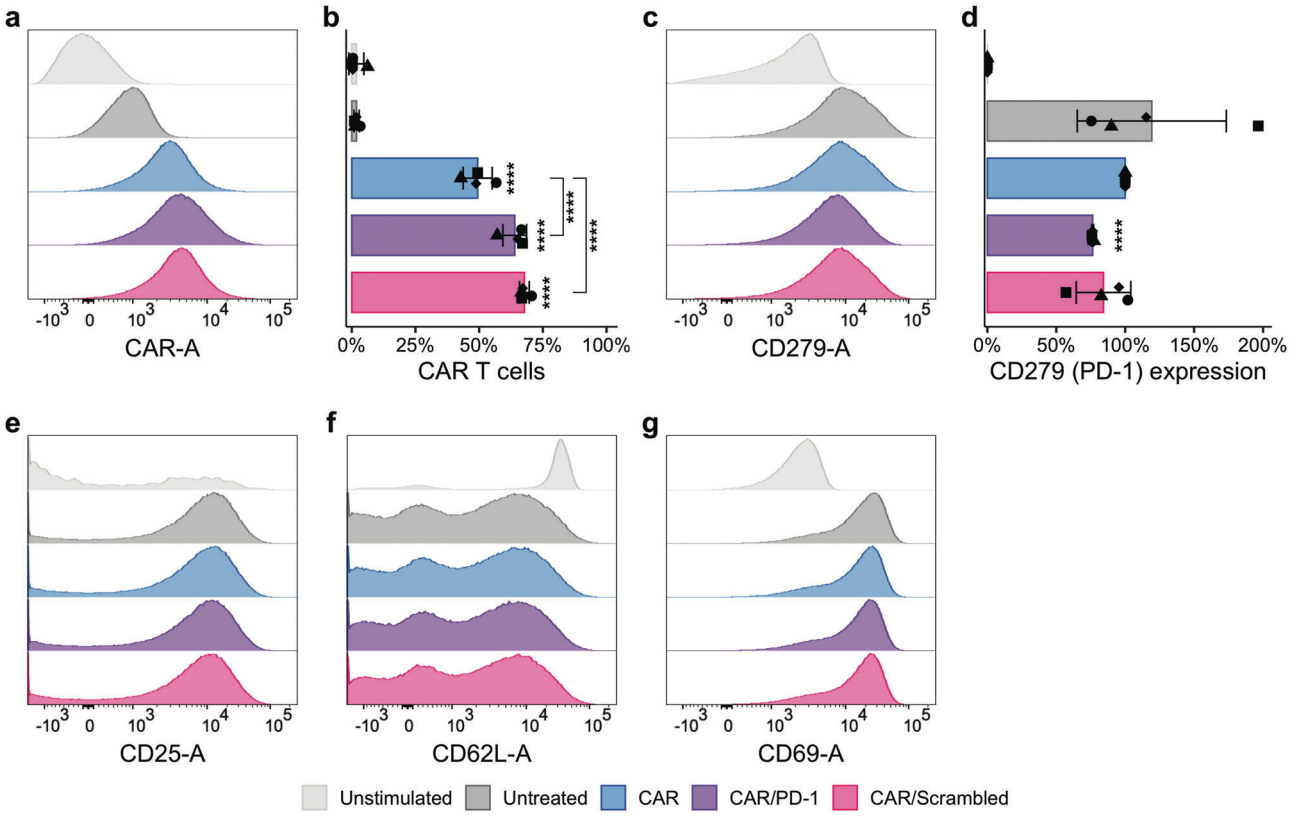

Figure 6. Representative histograms and bar plots demonstrating a,b) potent LNP-mediated CAR expression and c,d) LNP-mediated PD-1 knockdown following overnight activation and treatment with LNPs encapsulating CAR mRNA alone or CAR mRNA and either PD-1-targeting or scrambled siRNA at a dose of 500 ng of encapsulated mRNA per 100,000 cells. Representative histograms showing expression of activation markers e) CD25, f) CD62L (L-selectin), and g) CD69 in primary human T cells following activation and treatment with LNPs. ****: $p < 0.0001$. Statistical annotations without brackets represent comparisons to untreated T cells (b) or T cells treated only with CAR mRNA (d). Data are presented as mean ± standard deviation (data from $n = 4$ independent donors).

viable T cells, while cells treated with LNPs co-encapsulating CAR mRNA with PD-1 siRNA or scrambled siRNA displayed 64.0% ± 4.7% or 67.8% ± 1.9% transfection, respectively. We did not observe differential CAR expression in helper T cells versus cytotoxic T cells, suggesting uniform transfection of T cell subsets (Figure S11, Supporting Information). We also observed moderate PD-1 knockdown (Figure 6c–d). Interestingly, we saw a decrease in PD-1 expression relative to untreated cells for some donors when treating cells with LNPs containing only CAR mRNA. We observed a further decrease in PD-1 expression of 23.6% ± 0.7% when co-encapsulating CAR mRNA with PD-1 siRNA (Figure 6d). We did not observe any significant difference in PD-1 expression when treating cells with LNPs co-encapsulating CAR mRNA and scrambled siRNA compared to cells treated with CAR mRNA alone, suggesting that this knockdown is dependent on the sequence of the encapsulated siRNA, as expected. Moreover, expression levels of the activation markers CD25, CD62L, and CD69 appeared similar regardless of treatment, suggesting that inhibiting PD-1 expression did not cause changes to the activation state of CAR T cells during the CAR T generation process (Figure 6e–g). All told, these results demonstrate the utility of co-encapsulating siRNA alongside therapeutic mRNA and the ability to effectively deliver both cargoes in primary human T cells, enabling the ex vivo generation of therapeutically relevant "super" CAR T cells with transient immune checkpoint inhibition.

3. Conclusion

In this work, we developed an LNP platform for simultaneous gene expression and specific gene disruption in T cells. Co-encapsulating mRNA and siRNA in a single LNP formulation proved more potent for T cell delivery than encapsulating and delivering the cargoes separately. We selected a lead LNP candidate for its potent mRNA and siRNA delivery to Jurkat cells in vitro and employed this formulation to suppress PD-1 expression in primary human T cells, observing potent and fairly durable — but transient — knockdown alongside long-lived, strong exogenous mRNA expression, each detectable for at least one week. We then adapted our lead formulation to generate human CAR T cells with integrated immune checkpoint inhibition from primary cells ex vivo, noting improved CAR expression compared to mRNA-only LNPs and successful sequence-dependent PD-1 knockdown without changes to the overall activation state of the generated CAR T cells. We observed improved mRNA transfection even when using a scrambled siRNA sequence, consistent with a previous report and suggesting that the addition of siRNA — even in applications not strictly requiring RNAi — may benefit

mRNA LNP-based therapeutics broadly.[35] Potential future directions of this work include the silencing of other genes — including other immune checkpoint receptors like cytotoxic T-lymphocyte associated protein 4 (CTLA-4), lymphocyte activation gene 3 (LAG-3), and adenosine A_{2A} receptor (A2AR) but also other therapeutically relevant genes,[40] either alone or in combination — and extension to other therapeutic mRNAs such as engineered T cell receptors (TCRs) and cytokines, as well as other immune cell types.[41–43]

4. Eperimental Section

Ionizable Lipid Synthesis: C14-494 lipid was produced via a simple S_N2 addition chemistry as described previously.[32] Briefly, polyamine core 494 (Enamine, Monmouth Junction, NJ) was combined with excess 1,2-epoxytetradecane (MilliporeSigma, Burlington, MA) and ethanol in a glass scintillation vial under gentle stirring with a magnetic stir bar for 2 d at 80 °C. The resulting reaction mixture was dried using a Rotovap R-300 (Buchi, New Castle, DE), stored at 4 °C, and used for LNP formulation. Ionizable lipid identity and purity were confirmed using LC-MS.

Production of Reporter Gene mRNA Via IVT: Codon-optimized DNA sequences encoding either mCherry or EGFP were cloned into a proprietary mRNA production plasmid between a promoter for T7 RNA polymerase and a 101 nt poly(A) tail. RNA was transcribed using MegaScript T7 RNA polymerase (Thermo Fisher Scientific, Waltham, MA) with co-transcriptional capping using the CleanCap trinucleotide cap 1 analog (TriLink Biotechnologies, San Diego, CA), precipitated using lithium chloride, and purified using cellulose chromatography as described previously.[44] Uridine residues were fully substituted with N1-methylpseudouridine ($m^1\Psi$) by using N1-methylpsuedouridine-5'-triphosphate ($m^1\Psi$TP) (TriLink Biotechnologies) in the place of uridine-5'-triphosphate (UTP) in the reaction mixture. Resultant mRNA was analyzed by gel electrophoresis, sequenced, checked for dsRNA contaminants using a J2 dot blot, and stored frozen at −80 °C until use in LNP formulation.

LNP Formulation: All LNPs were formulated using microfluidic ethanol dilution as described previously.[33,34] Briefly, an ethanol phase was prepared containing ionizable lipid, helper lipid (DOPE and/or DSPC) (Avanti Polar Lipids, Birmingham, AL), cholesterol (MilliporeSigma), and 1,2-dimyristoyl-*sn*-glycero-3-phosphoethanolamine-N-[methoxy(polyethylene glycol)-2000] (C14-PEG2000) (Avanti Polar Lipids). An aqueous phase containing siRNA and/or mRNA in 10 mM citrate buffer at pH 3 (Thermo Fisher Scientific) was prepared separately. Ethanol and aqueous phases were then combined at a 1:3 volume ratio via microfluidic mixing in a device containing a staggered herringbone mixer architecture to produce LNPs. LNPs were dialyzed against 1× phosphate-buffered saline (PBS) (Thermo Fisher Scientific) for 2 h, filter sterilized using 0.22 µm filters (Genesee Scientific, San Diego, CA), and stored at 4 °C for later use.

Size and Zeta Potential: The size and polydispersity of each LNP formulation was measured using dynamic light scattering (DLS). Briefly, 10 µL of LNP suspension was diluted 100× in 1× PBS in disposable cuvettes (Fisher Scientific, Pittsburgh, PA). *z*-average diameter and PdI were then measured in triplicate using a ZetaSizer Nano (Malvern Panalytical, Malvern, Worcestershire, UK). Zeta potential was similarly measured in quintuplicate on a ZetaSizer Nano (Malvern Panalytical) after diluting LNPs 20× in deionized water in disposable cuvettes (VWR International, Radnor, PA). Data are reported as mean ± standard deviation ($n \geqslant 3$ measurements).

*Surface Ionization and **pKa***: LNP apparent p*Ka* was determined as described previously.[45] Briefly, a buffered solution consisting of 150 mM sodium chloride, 20 mM sodium phosphate, 20 mM ammonium acetate, and 25 mM ammonium citrate was adjusted to pH values ranging from 2 to 12 in increments of 0.5. 125 µL of each pH-adjusted solution and 5 µL of LNP formulation were plated in quadruplicate in a flat-bottom, black-walled 96-well plate. 2-(*p*-toluidino napthalene-6-sulfonic acid (TNS) was then added to each well to a final TNS concentration of 6 µM and fluorescence was read immediately on an Infinite 200 Pro microplate reader (Tecan Group, Männedorf, CH) at an excitation wavelength of 322 nm and an emission wavelength of 431 nm. The p*Ka* was taken as the pH corresponding to half-maximum fluorescence intensity (50% protonation).

RNA Entrapment and Concentration: Entrapment of RNA was assessed using a modified Quant-iT RiboGreen assay as described previously.[46] Briefly, LNP stocks were diluted 100× in tris-EDTA (TE) buffer or in 0.1% (v/v) Triton X-100 (MilliporeSigma) in TE buffer. 100 µL of diluted LNP was plated in quadruplicate in a flat-bottom, black-walled 96-well plate. 100 µL of working RiboGreen solution (Thermo Fisher Scientific) was added to each well. Fluorescence intensity was then read immediately on an Infinite 200 Pro microplate reader (Tecan Group) at an excitation wavelength of 480 nm and an emission wavelength of 520 nm. Entrapment was calculated as $1 - \frac{C_f}{C_t}$, where C_f was the RNA concentration in TE buffer (free RNA content in intact LNPs) and C_t was the RNA concentration with surfactant present (total RNA content in lysed sample). Resultant data are presented as mean ± standard deviation ($n = 4$ observations per LNP formulation). Total RNA content of LNPs was estimated using absorbance measurements at a wavelength of 260 nm on an Infinite 200 Pro (Tecan Group) or by inclusion of a standard curve produced by dilution of ribosomal RNA provided by the manufacturer in RiboGreen assays. siRNA and mRNA content were estimated by applying the ratios used for LNP formulation to total RNA content.

In Vitro RNA Delivery to Jurkat Cells: Jurkat immortalized human T cells stably expressing EGFP were a generous gift from Saar Gill at the University of Pennsylvania. Cells were cultured in Roswell Park Memorial Institute 1640 medium with *L*-glutamine supplemented with 10% (v/v) fetal bovine serum (FBS) and 1% (v/v) penicillin-streptomycin (RPMI). Cells were plated at 250,000 cells/well in 24-well plates in a volume of 500 µL. For excipient screens, cells were treated at a dose of 50 ng of mRNA per 100,000 cells. For cargo composition screens, cells were treated at doses of 2 ng of siRNA per 100,000 cells or 33.3 ng of mRNA per 100,000 cells. Flow cytometry experiments were conducted 24 h post-transfection.

Ex Vivo RNA Delivery to Primary Human T Cells — PD-1 Knockdown Kinetics Study: Primary human T cells from healthy volunteer donors were procured via the University of Pennsylvania Human Immunology Core (RRID:SCR_022380). $CD4^+$ and $CD8^+$ T cells were combined at a 1:1 ratio, plated at 100,000 cells/well in 100 µL of RPMI, and activated overnight using Dynabeads CD3/CD28 Human T-activator beads (Thermo Fisher Scientific) at a 1:1 bead:cell ratio. Following activation, cells were treated with LNPs at a dose of 300 ng of encapsulated mRNA per well. Immediately after treatment with LNPs and daily for 8 d thereafter, EGFP and PD-1 expression were measured via flow cytometry.

Ex Vivo RNA Delivery to Primary Human T Cells — Production of CAR mRNA via IVT: The gene sequence for a second-generation CAR targeting human CD19 was cloned into an in vitro transcription (IVT) plasmid between a T7 RNA polymerase promoter and a 64 nt poly(A) tail. CAR IVT plasmid was linearized immediately 3' of the poly(A) tail and transcription was performed using a HiScribe T7 High Yield RNA Synthesis Kit (New England Biolabs, Ipswich, MA) with full $m^1\Psi$ substitution accomplished by replacing the manufacturer-provided UTP with $m^1\Psi$TP (TriLink Biotechnologies). Transcripts were cleaned up using AMPure RNAClean XP beads (Beckman Coulter Life Sciences, Brea, CA), then capped using the Vaccinia capping system (New England Biolabs), with mRNA cap 2'-O-methyltransferase (New England Biolabs) used to generate a cap 1 structure. After a final bead cleanup, integrity of capped mRNA was verified via electrophoresis and mRNA was stored at −80 °C for later use.

Ex Vivo RNA Delivery to Primary Human T Cells — CAR-T Cell Generation and Fluorescence Microscopy: Primary human T cells were activated overnight in a well plate and treated with LNPs encapsulating CAR mRNA (either alone or with siRNA) at a dose of 500 ng of encapsulated mRNA per 100,000 cells. 24 h later, cells were rinsed with and resuspended in 1× PBS. 1 µg each of PD-1 primary antibody and biotinylated human CD19 (Sino Biological, Beijing, CN) was added to each sample and allowed to incubate at 4 °C for 15 min. Samples were rinsed and

resuspended in fresh PBS. 1 µg each of R-phycoerythrin (PE)-streptavidin conjugate (Sino Biological, Beijing, CN) and Alexa Fluor 488-conjugated secondary antibody was added to each sample and allowed to incubate at 4 °C for 15 min. After rinsing, cells were seeded on a chamber culture slide (Thermo Fisher Scientific) coated with poly-*L*-lysine (MilliporeSigma), fixed using 4% paraformaldehyde (MilliporeSigma), and counterstained with CellMask Deep Red (Thermo Fisher Scientific) and 4',6-diamidino-2-phenylindole (DAPI) (MilliporeSigma). ProLong Diamond antifade mountant (Thermo Fisher Scientific) was used to mount cover slips to prepared slides, which were then stored in the dark until imaging. Slides were imaged using a Leica Stellaris 5 microscope with a 20× objective. Image processing was performed using the Fiji image analysis software.[47]

Flow Cytometry: All flow cytometry was performed on an LSR II flow cytometer (BD, Franklin Lakes, NJ) equipped with violet, blue, green, and red lasers (RRID:SCR_022376). Clones and fluorophores used are listed in Table S1 (Supporting Information). For CAR staining, cells were incubated with 1 µg of biotinylated recombinant human CD19 (Sino Biological), then with 1 µg of streptavidin conjugated to Brilliant Violet 421 (BV421). For reporter gene assays and PD-1 knockdown kinetics studies, SYTOX Blue (Thermo Fisher Scientific) was used as a viability stain; for CAR/PD-1/activation studies, an annexin V conjugate was used instead to reduce spectral overlap (BioLegend). Compensation matrices for all experiments were obtained through the use of singly-stained compensation controls. Fluorescence-minus-one (FMO) controls were employed as necessary to establish background fluorescence levels for analysis. Standard gating methods were used with exclusion of doublets and nonviable cells. Representative gating schemes for all analyses are available in the Supporting Information (Figures S8,S9,S10). For expression of exogenous mRNA, gene expression was assessed as positivity rate; for siRNA-mediated knockdown, relative expression was assessed by comparing median fluorescence intensity (MFI) to appropriate controls in each experiment.

Statistical Analysis and Data Visualization: All statistical analysis and production of bar plots and characterization curves were performed in the R statistical programming language with a number of packages from the Comprehensive R Archive Network (CRAN).[48–58] The Nix package manager (with pinned `nixpkgs` revision `b7ce17b1e`) was used to manage all dependencies to maximize reproducibility.[59] Flow cytometry plots were produced using FlowJo 10 (BD, Franklin Lakes, NJ). Unless otherwise specified, statistical analysis was performed as a one-way analysis of variance (ANOVA) using post hoc two-tailed *t* tests with the Bonferroni-Holm correction for multiple comparisons. To control for potential changes in PD-1 expression following LNP treatment in CAR/PD-1/activation studies, PD-1 expression was normalized to cells treated with LNPs containing only CAR mRNA for each biological replicate. Consequently, one-sample *t* tests with the alternative hypothesis H_a: $\mu \neq 1$ were used to test for PD-1 knockdown, with the Bonferroni-Holm correction for multiple comparisons. All data are presented as mean ± standard deviation.

Supporting Information

Supporting Information is available from the Wiley Online Library or from the author.

Acknowledgements

M.J.M. acknowledges support from a US National Institutes of Health (NIH) Director's New Innovator Award (DP2 TR002776), a Burroughs Wellcome Fund Career Award at the Scientific Interface (CASI), a US National Science Foundation CAREER Award (CBET-2145491), an American Cancer Society Research Scholar Grant (RSG-22-122-01-ET), and the National Institutes of Health (NCI R01 CA241661, NCI R37 CA244911, and NIDDK R01 DK123049). A.G.H. and K.L.S. acknowledge support from the US National Science Foundation Graduate Research Fellowship (award number 1845298). M.M.B. acknowledges support US National Institutes of Health Ruth L. Kirschstein National Research Service Award (F31 CA260922). The content was solely the responsibility of the authors and did not necessarily represent the official views of the NIH.

Conflict of Interest

The authors declare no conflict of interest.

Author Contributions

A.G.H. and M.J.M. have filed a patent application related to this work. M.J.M. and M.M.B. are inventors on on a patent related to this work filed by the Trustees of the University of Pennsylvania (PCT/US20/56252). D.W. is an inventor on several patents related to this work filed by the Trustees of the University of Pennsylvania (11/990,646; 13/585,517; 13/839,023; 13/839,155; 14/456,302; 15/339,363; 16/299,202). N.C.S. holds equity in Fate Therapeutics, Tmunity Therapeutics, and Pfizer. N.C.S. is a scientific advisor for Immunai and Outpace Bio. C.H.J. has received grant support from Novartis and has patents related to CAR therapy with royalties paid from Novartis to the University of Pennsylvania. C.H.J. is a scientific cofounder and holds equity in Capstan Therapeutics and Tmunity Therapeutics. C.H.J. serves on the board of AC Immune and is a scientific advisor to Alaunos, BluesphereBio, Cabaletta, Carisma, Cartography, Cellares, Cellcarta, Celldex, Danaher, Decheng, ImmuneSensor, Poseida, Verismo, Viracta, and WIRB-Copernicus group.

Data Availability Statement

The data that support the findings of this study are available from the corresponding author upon reasonable request.

Keywords

checkpoint receptors, chimeric antigen receptors, immunotherapy, lipid nanoparticles, mRNA, RNA, siRNA

Received: June 9, 2023
Revised: August 13, 2023
Published online:

[1] M. P. Jogalekar, R. L. Rajendran, F. Khan, C. Dmello, P. Gangadaran, B.-C. Ahn, *Front. Immunol.* **2022**, *13*, 925985.
[2] E. Zmievskaya, A. Valiullina, I. Ganeeva, A. Petukhov, A. Rizvanov, E. Bulatov, *Biomedicines* **2021**, *9*, 59.
[3] FDA approval brings first gene therapy to the United States, https://www.fda.gov/news-events/press-announcements/fda-approval-brings-first-gene-therapy-united-states (accessed: August 2017).
[4] N. Bouchkouj, Y. L. Kasamon, R. A. de Claro, B. George, X. Lin, S. Lee, G. M. Blumenthal, W. Bryan, A. E. McKee, R. Pazdur, *Clin. Cancer Res.* **2019**, *25*, 1702.
[5] FDA Approves First Cell-Based Gene Therapy for Adult Patients with Multiple Myeloma, https://www.fda.gov/news-events/press-announcements/fda-approves-first-cell-based-gene-therapy-adult-patients-multiple-myeloma (accessed: March 2021).
[6] Y. Zhang, Z. Zhang, Y. Ding, Y. Fang, P. Wang, W. Chu, Z. Jin, X. Yang, J. Wang, J. Lou, Q. Qian, *J. Cancer Res. Clin. Oncol.* **2021**, *147*, 3725.
[7] D. M. O'Rourke, M. P. Nasrallah, A. Desai, J. J. Melenhorst, K. Mansfield, J. J. D. Morrissette, M. Martinez-Lage, S. Brem, E. Maloney, A. Shen, R. Isaacs, S. Mohan, G. Plesa, S. F. Lacey, J.-M. Navenot, Z. Zheng, B. L. Levine, H. Okada, C. H. June, J. L. Brogdon, M. V. Maus, *Sci. Trans. Med.* **2017**, *9*, 399.

[8] C. R. Maldini, D. T. Claiborne, K. Okawa, T. Chen, D. L. Dopkin, X. Shan, K. A. Power, R. T. Trifonova, K. Krupp, M. Phelps, V. D. Vrbanac, S. Tanno, T. Bateson, G. J. Leslie, J. A. Hoxie, C. L. Boutwell, J. L. Riley, T. M. Allen, *Nat. Med.* **2020**, *26*, 1776.
[9] B. Liu, W. Zhang, B. Xia, S. Jing, Y. Du, F. Zou, R. Li, L. Lu, S. Chen, Y. Li, Q. Hu, Y. Lin, Y. Zhang, Z. He, X. Zhang, X. Chen, T. Peng, X. Tang, W. Cai, T. Pan, L. Li, H. Zhang, *J. Clin. Investig.* **2021**, *131*, 19.
[10] J. G. Rurik, I. Tombácz, A. Yadegari, P. O. M. Fernández, S. V. Shewale, L. Li, T. Kimura, O. Y. Soliman, T. E. Papp, Y. K. Tam, B. L. Mui, S. M. Albelda, E. Puré, C. H. June, H. Aghajanian, D. Weissman, H. Parhiz, J. A. Epstein, *Sci.* **2022**, *375*, 91.
[11] D. Han, Z. Xu, Y. Zhuang, Z. Ye, Q. Qian, *J. Cancer* **2021**, *12*, 326.
[12] M. D. Gholami, G. A. kardar, Y. Saeedi, S. Heydari, J. Garssen, R. Falak, *Cell. Immunol.* **2017**, *322*, 1.
[13] N. N. Shah, T. J. Fry, *Nat. Rev. Clin. Oncol.* **2019**, *16*, 372.
[14] F. K. Dermani, P. Samadi, G. Rahmani, A. K. Kohlan, R. Najafi, *J. Cell. Physiol.* **2019**, *234*, 1313.
[15] L. Cherkassky, A. Morello, J. Villena-Vargas, Y. Feng, D. S. Dimitrov, D. R. Jones, M. Sadelain, P. S. Adusumilli, *J. Clin. Invest.* **2016**, *126*, 3130.
[16] A. P. R. Bally, J. W. Austin, J. M. Boss, *J. Immunol.* **2016**, *196*, 2431.
[17] K. C. Ohaegbulam, A. Assal, E. Lazar-Molnar, Y. Yao, X. Zang, *Trends Mol. Med.* **2015**, *21*, 24.
[18] H. O. Alsaab, S. Sau, R. Alzhrani, K. Tatiparti, K. Bhise, S. K. Kashaw, A. K. Iyer, *Front. Pharmacol.* **2017**, *8*, 561.
[19] E. McGowan, Q. Lin, G. Ma, H. Yin, S. Chen, Y. Lin, *Biomed. Pharmacother.* **2020**, *121*, 109625.
[20] N. Budimir, G. D. Thomas, J. S. Dolina, S. Salek-Ardakani, *Cancer Immunol. Res.* **2022**, *10*, 146.
[21] J. R. Kuchroo, D. A. Hafler, A. H. Sharpe, L. E. Lucca, *Sci. Immunol.* **2021**, *6*, eabf4034.
[22] L. J. Rupp, K. Schumann, K. T. Roybal, R. E. Gate, C. J. Ye, W. A. Lim, A. Marson, *Sci. Rep.* **2017**, *7*, 737.
[23] W. Hu, Z. Zi, Y. Jin, G. Li, K. Shao, Q. Cai, X. Ma, F. Wei, *Cancer Immunol., Immunother.* **2019**, *68*, 365.
[24] X. Liu, Y. Zhang, C. Cheng, A. W. Cheng, X. Zhang, N. Li, C. Xia, X. Wei, X. Liu, H. Wang, *Cell Res.* **2017**, *27*, 154.
[25] S. Rafiq, O. O. Yeku, H. J. Jackson, T. J. Purdon, D. G. van Leeuwen, D. J. Drakes, M. Song, M. M. Miele, Z. Li, P. Wang, S. Yan, J. Xiang, X. Ma, V. E. Seshan, R. C. Hendrickson, C. Liu, R. J. Brentjens, *Nat. Biotechnol.* **2018**, *36*, 847.
[26] M. M. Billingsley, N. Singh, P. Ravikumar, R. Zhang, C. H. June, M. J. Mitchell, *Nano Lett.* **2020**, *20*, 1578.
[27] M. M. Billingsley, A. G. Hamilton, D. Mai, S. K. Patel, K. L. Swingle, N. C. Sheppard, C. H. June, M. J. Mitchell, *Nano Lett.* **2021**, *22*, 533.
[28] M. A. Oberli, A. M. Reichmuth, J. R. Dorkin, M. J. Mitchell, O. S. Fenton, A. Jaklenec, D. G. Anderson, R. Langer, D. Blankschtein, *Nano Lett.* **2016**, *17*, 1326.
[29] M. Jayaraman, S. M. Ansell, B. L. Mui, Y. K. Tam, J. Chen, X. Du, D. Butler, L. Eltepu, S. Matsuda, J. K. Narayanannair, K. G. Rajeev, I. M. Hafez, A. Akinc, M. A. Maier, M. A. Tracy, P. R. Cullis, T. D. Madden, M. Manoharan, M. J. Hope, *Angew. Chem.* **2012**, *124*, 8657.
[30] K. A. Whitehead, J. R. Dorkin, A. J. Vegas, P. H. Chang, O. Veiseh, J. Matthews, O. S. Fenton, Y. Zhang, K. T. Olejnik, V. Yesilyurt, D. Chen, S. Barros, B. Klebanov, T. Novobrantseva, R. Langer, D. G. Anderson, *Nat. Commun.* **2014**, *5*, 1.
[31] K. L. Swingle, A. G. Hamilton, M. J. Mitchell, *Trends Mol. Med.* **2021**, *27*, 616.
[32] K. J. Kauffman, J. R. Dorkin, J. H. Yang, M. W. Heartlein, F. DeRosa, F. F. Mir, O. S. Fenton, D. G. Anderson, *Nano Lett.* **2015**, *15*, 7300.
[33] D. Chen, K. T. Love, Y. Chen, A. A. Eltoukhy, C. Kastrup, G. Sahay, A. Jeon, Y. Dong, K. A. Whitehead, D. G. Anderson, *J. Am. Chem. Soc.* **2012**, *134*, 6948.
[34] S. J. Shepherd, C. C. Warzecha, S. Yadavali, R. El-Mayta, M.-G. Alameh, L. Wang, D. Weissman, J. M. Wilson, D. Issadore, M. J. Mitchell, *Nano Lett.n* **2021**, *21*, 5671.
[35] R. L. Ball, K. A. Hajj, J. Vizelman, P. Bajaj, K. A. Whitehead, *Nano Lett.* **2018**, *18*, 3814.
[36] X. Han, H. Zhang, K. Butowska, K. L. Swingle, M.-G. Alameh, D. Weissman, M. J. Mitchell, *Nat. Commun.* **2021**, *12*, 7233.
[37] X. Hou, T. Zaks, R. Langer, Y. Dong, *Nat. Rev. Mater.* **2021**, *6*, 1078.
[38] R. T. Abraham, A. Weiss, *Nat. Rev. Immunol.* **2004**, *4*, 301.
[39] E. A. Sarnoski, R. Song, E. Ertekin, N. Koonce, M. Acar, *iScience* **2018**, *7*, 96.
[40] D. Mai, O. Johnson, J. Reff, T.-J. Fan, J. Scholler, N. C. Sheppard, C. H. June, *Proc. Natl. Acad. Sci. U.S.A.* **2023**, *120*, e2218632120.
[41] A. C. Anderson, N. Joller, V. K. Kuchroo, *Immunity* **2016**, *44*, 989.
[42] S. Qin, L. Xu, M. Yi, S. Yu, K. Wu, S. Luo, *Mol. Cancer* **2019**, *18*, 155.
[43] L. Giuffrida, K. Sek, M. A. Henderson, J. Lai, A. X. Y. Chen, D. Meyran, K. L. Todd, E. V. Petley, S. Mardiana, C. Mølck, G. D. Stewart, B. J. Solomon, I. A. Parish, P. J. Neeson, S. J. Harrison, L. M. Kats, I. G. House, P. K. Darcy, P. A. Beavis, *Nat. Commun.* **2021**, *12*, 3236.
[44] M. Baiersdörfer, G. Boros, H. Muramatsu, A. Mahiny, I. Vlatkovic, U. Sahin, K. Karikó, *Mol. Ther. Nucleic Acids* **2019**, *15*, 26.
[45] K. A. Hajj, R. L. Ball, S. B. Deluty, S. R. Singh, D. Strelkova, C. M. Knapp, K. A. Whitehead, *Small* **2019**, *15*, 1805097.
[46] K. L. Swingle, H. C. Safford, H. C. Geisler, A. G. Hamilton, A. S. Thatte, M. M. Billingsley, R. A. Joseph, K. Mrksich, M. S. Padilla, A. A. Ghalsasi, M.-G. Alameh, D. Weissman, M. J. Mitchell, *J. Am. Chem. Soc.* **2023**, *145*, 4691.
[47] J. Schindelin, I. Arganda-Carreras, E. Frise, V. Kaynig, M. Longair, T. Pietzsch, S. Preibisch, C. Rueden, S. Saalfeld, B. Schmid, J.-Y. Tinevez, D. J. White, V. Hartenstein, K. Eliceiri, P. Tomancak, A. Cardona, *Nat. Methods* **2012**, *9*, 676.
[48] R Core Team, *R: A Language and Environment for Statistical Computing*, R Foundation for Statistical Computing, Vienna, Austria **2022**. https://www.R-project.org/
[49] D. Robinson, A. Hayes, S. Couch, *broom: Convert Statistical Objects into Tidy Tibbles*, **2022**, https://CRAN.R-project.org/package=broom, R package version 1.0.1.
[50] H. Wickham, R. François, L. Henry, K. Müller, *dplyr: A Grammar of Data Manipulation*, **2022**, https://CRAN.R-project.org/package=dplyr, R package version 1.0.10.
[51] H. Wickham, *forcats: Tools for Working with Categorical Variables (Factors)*, **2022**, https://CRAN.R-project.org/package=forcats, R package version 0.5.2.
[52] E. Clarke, S. Sherrill-Mix, *ggbeeswarm: Categorical Scatter (Violin Point) Plots*, **2017**, https://CRAN.R-project.org/package=ggbeeswarm, R package version 0.6.0.
[53] H. Wickham, *ggplot2: Elegant Graphics for Data Analysis*, Springer-Verlag, New York **2016**.
[54] B. M. Greenwell, C. M. S. Kabban, *R J.* **2014**, *6*, 90.
[55] J. Ooms, *magick: Advanced Graphics and Image-Processing in R*, **2021**, https://CRAN.R-project.org/package=magick, R package version 2.7.3.
[56] T. L. Pedersen, *patchwork: The Composer of Plots*, **2022**, https://CRAN.R-project.org/package=patchwork, R package version 1.1.2.
[57] H. Wickham, J. Bryan, *readxl: Read Excel Files*, **2022**, https://CRAN.R-project.org/package=readxl, R package version 1.4.1.
[58] H. Wickham, M. Girlich, *tidyr: Tidy Messy Data*, **2022**, https://CRAN.R-project.org/package=tidyr, R package version 1.2.1.
[59] E. Dolstra, The purely functional software deployment model, Institute for Programming research and Algorithmics, **2006**.